Experiments on optical fiber interferometers and laser modes

Miguel V. Andrés and Oswaldo Contreras
Departamento de Física Aplicada, Universidad de Valencia, 46100 Burjasot, Valencia, Spain

(Received 13 March 1991; accepted 11 November 1991)

Three experiments on optical fiber interferometers, suitable for a teaching laboratory, are described. The guiding characteristics of single mode optical fibers enable simple interferometry experiments with large path differences to be carried out easily. These experiments show that the fringe visibility exhibits a periodic dependence on the path difference when using a multilongitudinal mode HeNe laser. A simple model can be used to explain this dependence in terms of the mode spectrum of the laser.

I. INTRODUCTION

Optical fiber applications in sensing and signal processing[1-5] have grown during the last decade. However, the undergraduate students show a lack of familiarity with experiments connected with those applications. At present, some basic experiments suitable for an undergraduate physics laboratory have been developed,[6] including a simple fiber interferometer experiment. Two optical fiber sensor experiments based on amplitude modulation of the signal[7] have been fully described as well.

A number of applications in sensing and signal processing rely on optical fiber interferometers. We describe here a set of three experiments, which can provide a good knowledge of the techniques and the physics involved in an optical fiber interferometer. These experiments show the advantage of using single mode fiber to perform interferometry experiments with large path differences, which would require special skills if bulk optics had to be used. This advantage relies on the guided propagation of the light within the fiber, which avoids the difficulties with careful alignment of mirrors and isolation from vibrations.

The characteristics of an interferometric system will depend on the coherence properties of the source. To start with, we can say that to give rise to interference, the coherence length has to be of the same order as the path difference. However, when using a multimode gas laser the notion of coherence length is more subtle. A simple theoretical analysis[8] shows that multimode lasers can be used with large path interferometers, but the visibility of the interferometric fringes will exhibit some periodic dependence on the path difference. This dependence is determined by the mode spectrum of the laser.

The results of three different experiments are described in this paper. The first two are optical fiber interferometers, one with the structure of a Fabry–Perot interferometer and the other with the structure of a Michelson interferometer. We investigate, in both cases, the dependence of the fringe visibility on the path difference. A third experiment consists of an optical fiber ring resonator, which is used to provide direct observation of the mode spectrum of the laser. The knowledge of the mode spectrum is required to provide a detailed explanation of the results of the other experiments; otherwise only a qualitative explanation can be given. However, this third experiment is not necessary for the other two and, since it is more complex to perform and to understand, it should be left for the more skilled students. If this experiment is not carried out, then the average mode spectrum of the laser can be worked out from its specifications, as described in Sec. II C.

Before carrying out these experiments, it should be useful for the students to get some experience on the polarization properties and polarization controllers[9] in single mode optical fibers. An optical fiber interferometer always requires some polarization control to make sure that the signals interfere matching their polarizations. That requirement can be fulfilled using polarization preserving fiber carefully aligned or, alternatively, using standard low birefringent fiber and providing a suitable polarization control. The correct polarization matching corresponds to maximum visibility of the interferometric fringes, which can be used as a reference for the adjustment of the polarization controller. Although it is simple to construct a polarization controller in a machine shop following the design rules given in Ref. 9, one can perform a satisfactory polarization control by bending and twisting a portion of the fiber of about 30 cm. Once the visibility is adjusted to its maximum then the fiber should be held with any available thing, e.g., bits of sticking tape.

Single mode fiber operating at 633 nm is available from different manufacturers. The fiber that we have used was provided by Lightwave Technology Inc. (fiber model F1506C, $3 per meter) and has a core diameter of about 5 μm, a cladding diameter of 125 μm and is made of fused silica.

II. EXPERIMENTS

A. Fabry–Perot interferometer

Figure 1 gives the experimental arrangement used for measuring the fringe visibility of an optical fiber Fabry–Perot. The optical source is a polarized HeNe laser, 633-nm, 5-mW, Spectra-Physics model 105P. A piece of single mode fiber, of about 3 m, defines a low finesse Fabry–Perot, since no coating or mirrors are attached to the fiber ends A and B. In fact the finesse is about 2 and the system can be regarded as a two beam interferometer, the first beam being the signal reflected back at A, and the second beam the signal reflected at B and transmitted through A. Due to the low reflection at the interface silica/air, the higher-order reflections can be neglected. A standard silicon photodiode with a current-to-voltage transducer is used to measure the intensity of the signal reflected from the Fabry–Perot.

In order to scan several fringes of the interferometer to enable measurement of the visibility, a piezoelectric cylinder was included in the experimental arrangement (Fig. 1). In our experiments we have used a Vernitron tube, part No. 32-32200-5H, of 50.8-mm length, 50.8-mm diameter, and 5-mm wall thickness, and about 1 m of fiber was

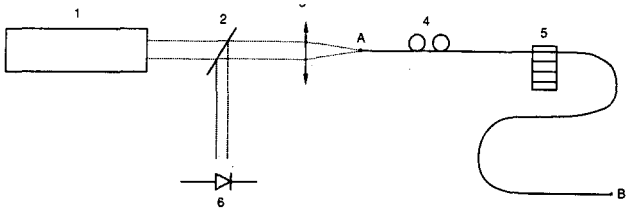

Fig. 1. Optical fiber Fabry–Perot interferometer: (1) laser, (2) splitter, (3) microscope objective, (4) polarization controller, (5) piezoelectric cylinder, (6) photodiode, (AB) single mode fiber.

wound round the tube. We scan several fringes driving the piezoelectric cylinder with a low-frequency triangular signal of 15-V amplitude. However, a number of alternative methods can be used to scan several fringes, e.g., binding the fiber to a loudspeaker and driving it with an audio amplifier.

The measurements were performed as a function of the fiber length by repeatedly cutting off the end B with a standard cleaver, model Newport F-BK1, after removing the UV-curable coating with paint stripper. Every time that the fiber was cut, we measured the length of the individual piece of fiber cut from the end B, δX, and the maximum and minimum levels of an interferometric fringe, $I_{\max}$ and $I_{\min}$. It has to be mentioned that the values of $I_{\max}$ and $I_{\min}$ may exhibit a slow drift. This drift can be observed for the cases with smaller visibility, i.e., the cases with lower difference $I_{\max} - I_{\min}$. In such cases we have measured the values of $I_{\max}$ and $I_{\min}$ corresponding to the time intervals that showed higher visibility. The origin and characteristics of that drift will be explained is Secs. II C and III.

The measurements of $I_{\max}$, $I_{\min}$, and δX have been used to calculate the visibility $V = (I_{\max} - I_{\min})/(I_{\max} + I_{\min})$, the average level of the signal $I_{\text{av}} = (I_{\max} + I_{\min})/2$, and the total length of fiber that has been cut, $X = \Sigma \delta X$.

Figure 2 shows the calculated visibility as a function of X. We observe that the visibility exhibits certain random variations mixed with a smooth and periodic dependence on X. Figure 3 shows the average level of the signal as a function of X. This figure provides some useful information to check the quality of the cleaving technique. Imperfectly cleaved ends produce low values of I_{av}, since the intensity of the signal reflected at those ends will be lower than what is expected for a silica/air interface. Small and smooth fluctuations of I_{av} can be explained in terms of power fluctuations of the laser source and mechanical drifts of the optical coupling system, but the larger fluctuations of I_{av} in Fig. 3 are due to the cleaving technique. Thus the experimental points of Fig. 2 can be filtered, defining a minimum acceptable value for I_{av}, which will be discussed in Sec. III.

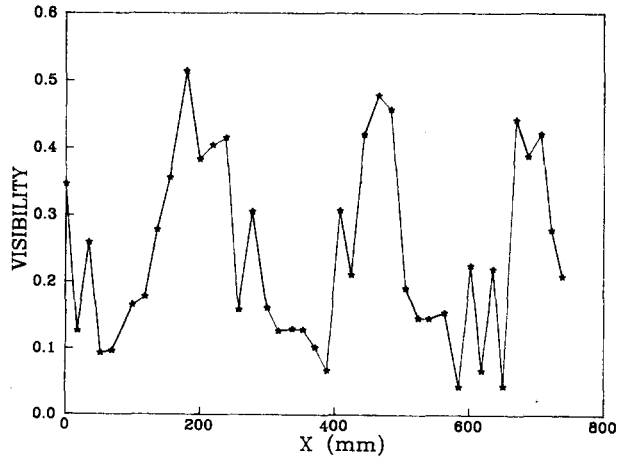

Fig. 2. Fringe visibility of an optical fiber Fabry–Perot as a function of the length of fiber cut off: (*) experimental points.

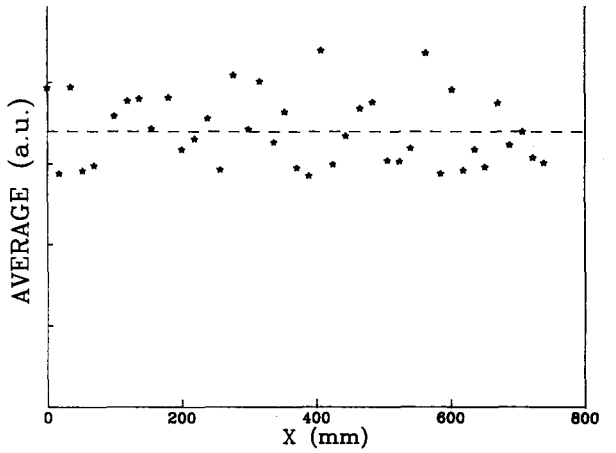

Fig. 3. Average intensity of an optical fiber Fabry–Perot as a function of the length of fiber cut off: (*) experimental points, (- - -) minimum value selected to fit Eq. (12) (see Fig. 9 in Sec. III).

B. Michelson interferometer

Figure 4 gives the experimental setup of an optical fiber Michelson interferometer based on a 50:50 coupler. The coupler was made in our own laboratory using a simple fusion-pulling technique, but any standard 50:50 single mode coupler will work. However, it is advisable to use a coupler made of the same type of single mode fiber as the fiber that is spliced to be cut back (e.g., SIFAM Ltd. manufactures single mode couplers using Lightwave Technology F1506C fiber). In our setup, a reusable GTE Lab splice (about $5) was used to splice the fiber pigtail of the coupler to a piece of fiber of about 1.5 m (label 7 in Fig. 4). The laser, the coupling optics, the piezoelectric cylinder and the detector are as described for Fig. 1. The signal reaching the detector is the interference between the two signals reflect-

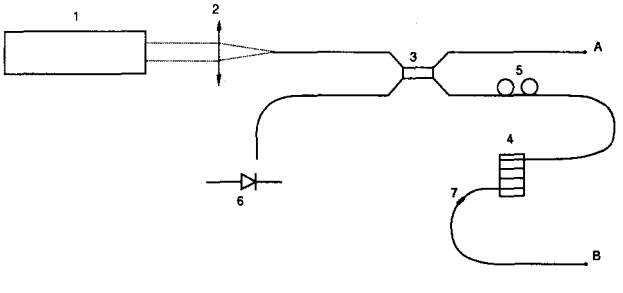

Fig. 4. Optical fiber Michelson interferometer: (1) laser, (2) microscope objective, (3) coupler, (4) piezoelectric cylinder, (5) polarization controller, (6) photodiode, (7) splice.

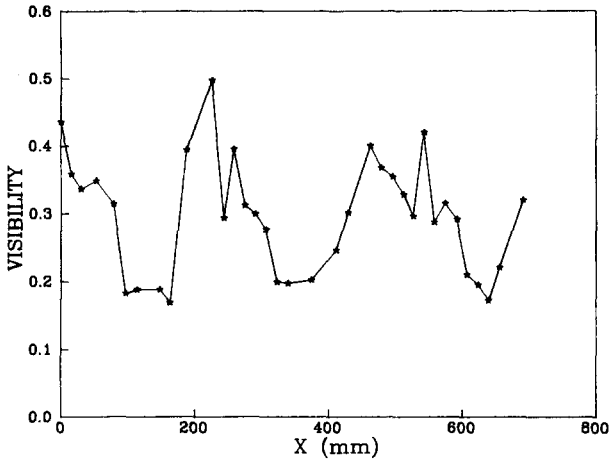

Fig. 5. Fringe visibility of an optical fiber Michelson as a function of the length of fiber cut off: (*) experimental points.

ed back at points A and B. In our experiment the path difference between the two arms ending at points A and B was about 2.5 m.

The maximum and minimum levels of the interferometric fringes were measured as a function of the path difference by repeatedly cutting off the fiber end B. The results of those measurements, V and I_{av}, are given in Figs. 5 and 6. The calculated visibility V again shows a periodic dependence on X mixed up with random variations. As before, the fluctuations of I_{av} are due to the cleaving technique. Thus Fig. 6 can be used to identify the worst cleaved ends and to filter the experimental points of Fig. 5, as will be done in Sec. III.

C. Ring interferometer

Figure 7 is a diagram of our experimental setup for direct observation of the mode spectrum of the laser, using an optical fiber ring resonator. Now again, we have used a coupler made in our own laboratory. However, we have repeated the experiment using a standard 90:10 single mode coupler manufactured by SIFAM Ltd., and that system gave the same results. The characteristics of this interferometer[10] can be compared with the signal reflected from a bulk Fabry–Perot, and therefore can effectively be used to observe the mode spectrum of a laser. Figure 8 shows three different recorded outputs, which were taken at time intervals of a few minutes. The top trace in each plot is the triangular modulation applied to the piezoelectric cylinder, which scans an interval of 1.83 wavelengths, i.e., a phase delay of 11.5 rad. The bottom trace is the signal detected by the photodiode at the output fiber, where every resonance of the system produces a dip at the output. If single mode fiber is used and the polarization controller is adjusted to avoid splitting of the resonances, then every peak observed at the output will correspond to a different wavelength of the source, i.e., a different mode of the laser.

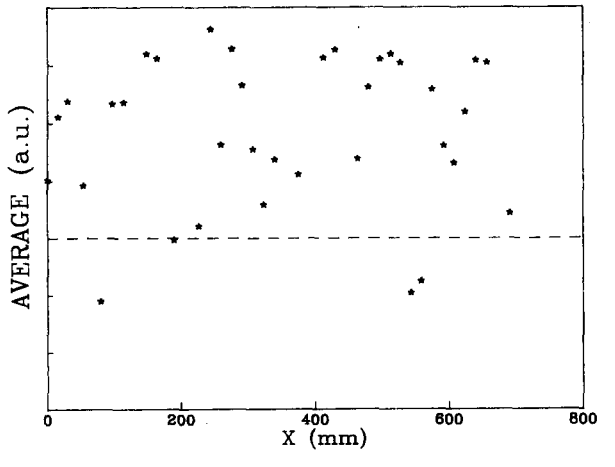

Fig. 6. Average intensity of an optical fiber Michelson as a function of the length of fiber cut off: (*) experimental points, (- - -) minimum value selected to fit Eq. (12) (see Fig. 10 in Sec. III).

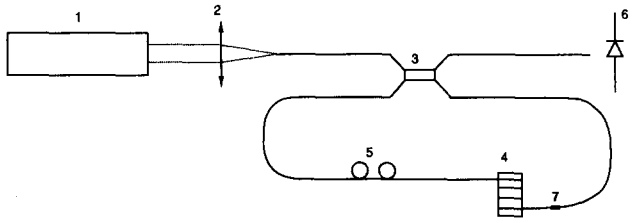

Fig. 7. Optical fiber ring interferometer: (1) laser, (2) microscope objective, (3) coupler, (4) piezoelectric cylinder, (5) polarization controller, (6) photodiode, (7) splice.

To identify the different modes of the laser from Fig. 8 requires a careful analysis. The modulating signal applied to the piezoelectric cylinder will give rise to identical outputs every 2π rad, therefore the scale factor for horizontal distances on the plots can be easily determined. The number of resonances within that interval gives the number of modes, which is three for our laser, although sometimes only two are observed.

This result could be worked out from the data provided by the manufacturer, who specifies that the laser has a single transverse mode, TEM_{00}, with a longitudinal mode spacing $\delta f = 413$ MHz. Since the width of the gain curve for a HeNe laser is about 1500 MHz, only three or two longitudinal cavity modes will lie within the gain curve. These modes will exhibit enough gain to oscillate.[11] Therefore, our laser is likely to exhibit three or two modes. In fact, this conclusion obtained from the laser specifications can be used to discuss the results of the previous experiments. Therefore, this third experiment is not necessary for the first two experiments, as was already mentioned in the Introduction.

The mode spacing δf determines the effective length of the laser cavity L:

$$L = c/2\delta f. \tag{1}$$

Thus the nominal value $\delta f = 413$ MHz gives $L = 0.363$ m.

The central mode of the mode spectrum can be identified, for example in Fig. 8(a), by looking for a resonance with two symmetrically separated adjacent resonances. The central mode corresponds to the strongest resonance in Fig. 8(a) and (b), as expected. The phase difference between the central mode and one of the adjacent modes ϕ is determined by the total length l of the fiber ring:

$$l = (2L/n)(m + \phi/2\pi), \tag{2}$$

where n is the effective refractive index of the fiber and m is an integer. In our case $\Phi/2\pi = 0.40$, and since $l \approx 1.1$ m, it leads to $m = 2$. This allows for an accurate determination

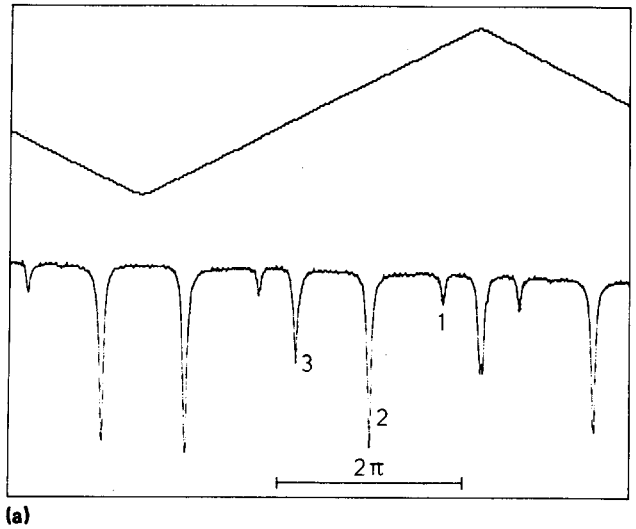

(a)

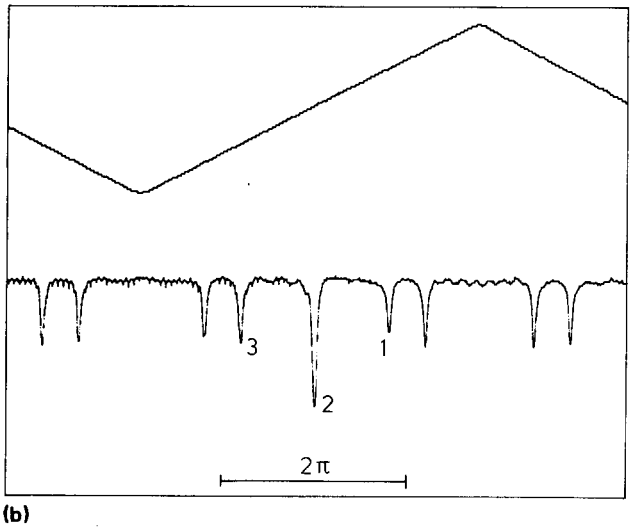

(b)

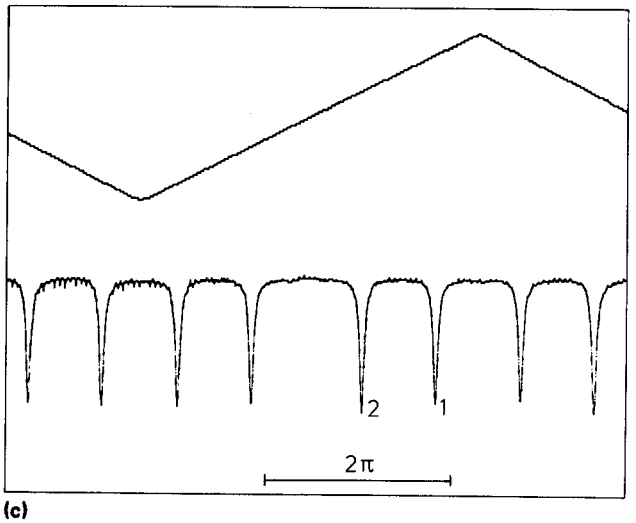

(c)

Fig. 8. Output signal of an optical fiber ring interferometer: the top trace is the phase modulating signal and the bottom trace is the signal recorded at the output fiber. (a), (b), and (c): three different records.

of the fiber length l. If we take $n = 1.46$ and $m = 2$, then Eq. (2) gives $l = 1.19$ m.

The relative intensities of each mode evolved slowly with time. Typically two modes dominated the laser output, as Fig. 8(a) and (c) show. Figure 8(b) shows that sometimes it was possible to observe two secondary modes with similar intensities, around a dominant central mode. These changes of the relative intensities of each mode are due to instabilities of the laser cavity, mainly of thermal origin. Such instabilities generate a continuous drift of the cavity modes within the gain curve of the laser.

III. DISCUSSION

In this section we explain the results of experiments II A and II B in terms of a simple model,[8] taking into account the mode spectrum found in experiment II C.

Both experiments II A and II B can be described as the interference between the signals of intensities I_A and I_B reflected at points A and B of Figs. 1 and 3. If the laser radiation is modeled by a set of three longitudinal modes of intensities I_1, I_2, and I_3, and frequencies $f_1 = f - \delta f$, $f_2 = f$ and $f_3 = f + \delta f$, then the overall interference between I_A and I_B can be expressed as the superposition of the interference intensities of each mode, neglecting the spectral width of individual modes. The model assumes that each mode does not interfere with the others, since they are not phase correlated. If I_{Ai} and I_{Bi} for $i = 1,2,3$, are the signals reflected at points A and B for modes 1, 2 and 3, then the interference intensity P_i of mode i will be given by

$$P_i = (I_{Ai} + I_{Bi})[1 + q\cos\theta_i], \tag{3}$$

where q and θ_i are given by

$$q = 2\sqrt{I_{Ai}I_{Bi}}/(I_{Ai} + I_{Bi}), \tag{4}$$

$$\theta_i = (2\pi f_i/c)2nX_{AB}; \tag{5}$$

X_{AB} being the optical fiber length difference between the points A and B. This difference can be written as $X_0 - X$, where X_0 is the initial value of X_{AB} and X is the length of fiber cut off. The ratio I_{Bi}/I_{Ai} can be assumed to be common to all three modes, and both I_{Ai} and I_{Bi} proportional to I_i. Thus q will be independent of I_i, i.e., common to the three modes.

The resulting interference intensity P, after taking into account the three modes, will be given by

$$P = \sum_{i=1}^{i=3} P_i = I_{\text{av}} + \sum_{i=1}^{i=3} 2\sqrt{I_{Ai}I_{Bi}}\cos\theta_i, \tag{6}$$

where

$$I_{\text{av}} = \sum_{i=1}^{i=3} (I_{Ai} + I_{Bi}). \tag{7}$$

It has been shown[8] that the visibility V can be written as

$$V = A/I_{\text{av}}, \tag{8}$$

where

$$A^2 = q^2\left(\sum_{i=1}^{i=3} (I_{Ai} + I_{Bi})\sin\theta_i\right)^2 + q^2\left(\sum_{i=1}^{i=3} (I_{Ai} + I_{Bi})\cos\theta_i\right)^2, \tag{9}$$

which leads to

$$V^2 = q^2[a + b\cos\delta\theta + c\cos 2\delta\theta], \tag{10}$$

where:

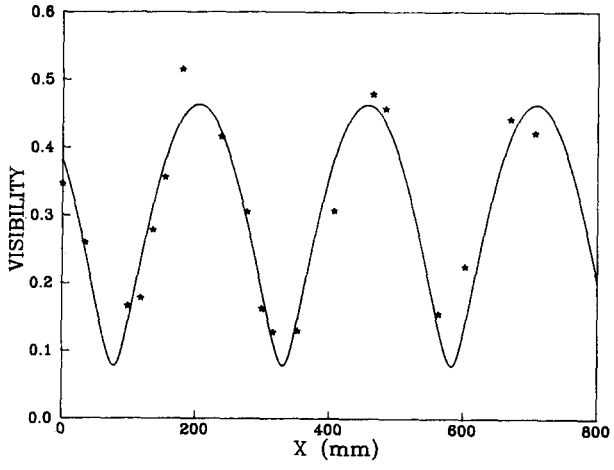

Fig. 9. Fringe visibility of an optical fiber Fabry–Perot as a function of the length of fiber cut off: (*) selected experimental points, (--) fit of Eq. (12).

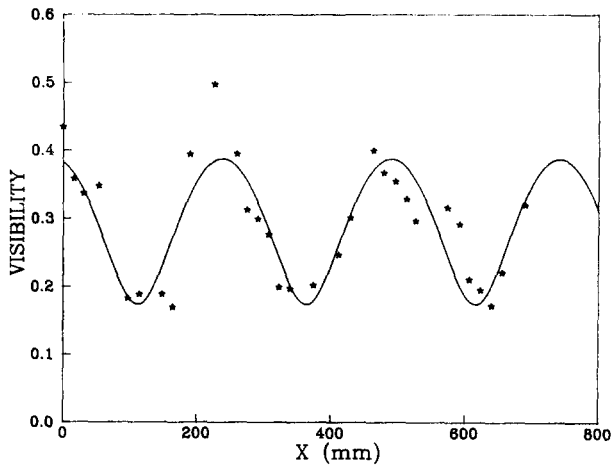

Fig. 10. Fringe visibility of an optical fiber Michelson as a function of the length of fiber cut off: (*) selected experimental points, (--) fit of Eq. (12).

$$a = 1 - b - c,$$
$$b = 2(I_1 I_2 + I_2 I_3)/(I_1 + I_2 + I_3)^2,$$
$$c = 2I_1 I_3/(I_1 + I_2 + I_3)^2, \qquad (11)$$
$$\delta\theta = 2\pi(n/L)X_{AB}.$$

Equation (10) shows that V^2, and therefore V as well, has a periodic dependence on the path difference X_{AB}, of periodicity L/n. This result is independent of the intensities of the longitudinal modes and can be shown to be independent of the number of modes. This result can be used to work out a first L/n experimental value from Figs. 2 and 5.

The details of how V^2 depends on X_{AB} are determined by the relative values of the intensities I_1, I_2, and I_3. Although experiment II.3 showed that those values were changing continuously with time, we can derive a useful approximation to Eq. (10) suitable for the results of experiments A and B. This approximation will lead to an accurate determination of L/n from Figs. 2 and 5. Since both I_1 and I_3 are smaller than I_2, we can neglect the third term in Eq. (10) and take:

$$V^2 \approx q^2(a + b\cos\delta\theta). \qquad (12)$$

Furthermore, we will consider that a and b remain constant with time. Although this final approximation is less accurate, it does give satisfactory results. To explain this, we have to consider first that for $\delta\theta \approx 0$, V exhibits its maximum value, $V_{\max} = q$, which happens to be always independent of the relative values of I_1, I_2, and I_3.

On the other hand, when $\delta\theta \approx \pi$, V exhibits its minimum value, $V^2_{\min} = q^2(1 - 2b)$, which will depend on the changes of the relative values of I_1, I_2, and I_3, through the coefficient b. Indeed, this agrees with the experimental fact that when one measures V in the experiments A and B it is possible to observe smooth variations of V with time, but only for the lowest values of V. The data recorded were the highest V values for a given X_{AB}, avoiding some eventual situations with $V = 0$ by simply waiting a certain time before recording the data. In other words, the data in Figs. 2 and 5 correspond to mode spectra as given by Figs. 8(a) and (b), while situations such as that shown in Fig. 8(c) ($I_1 = I_2, I_3 = 0$) that would give rise to $V_{\min} = 0$ were avoided.

Equation (12) determines the dependence of V on X. This equation does not take into account the effects of imperfectly cleaved ends. Therefore, if we want to check this equation with the results of Figs. 2 and 5, then the experimental points have to be filtered. We only have to take into account that in Sec. II we mentioned that the points with lower I_{av} were those with worst cleaved ends. The procedure that we followed was to remove from Figs. 2 and 5 the points with lower I_{av} (see Figs. 3 and 6) up to observing a smooth enough dependence of V on X. Figures 9 and 10 give the selected points from Figs. 2 and 5 after removing the points with I_{av} lower than the values defined by the dashed lines in Figs. 3 and 6.

The experimental V values given in Figs. 9 and 10 do reasonably follow Eq. (12). A mean square fitting of Eq. (12) gave the values $q^2a = 0.110$, $q^2b = 0.104$, $L/n = 0.252$ m, and $X_0 = 2.976$ m for Fig. 9, and $q^2a = 0.090$, $q^2b = 0.061$, $L/n = 0.252$ m, and $X_0 = 2.506$ m for Fig. 10. Since $L = 0.363$ m, we conclude that $n = 1.44$ for our silica fiber, which is a reasonable result.

IV. CONCLUSION

Three experiments on optical fiber interferometers have been discussed, taking into account the mode spectrum of the laser. These experiments can provide the basis of a good understanding of the techniques and physics involved in optical fiber interferometers, and can motivate students to develop their own projects on optical fiber sensors and signal processing systems, based on such interferometers.

ACKNOWLEDGMENTS

The authors are grateful to K. W. H. Foulds and A. E. Ennos for their useful suggestions. Acknowledgments for financial support are made to the DGICYT of Spain (Grant PB88-0346).

[1] J. Dakin and B. Culshaw, *Optical Fiber Sensors, Volume I: Principles and Components, Volume II: Systems and Applications* (Artech House, London, 1988 and 1989).

[2] B. Culshaw, *Optical Fibre Sensing and Signal Processing* (Peregrinus, London, 1984).

[3] G. D. Pitt, P. Extance, R. C. Neat, D. N. Batchelder, R. E. Jones, J. A. Barnett, and R. H. Pratt, "Optical-fibre sensors," IEE Proc. **132**, 214–248 (1985).
[4] T. G. Giallorenzi, J. A. Bucaro, A. Dandridge, G. H. Sigel, JR., J. H. Cole, S. C. Rashleigh, and R. G. Priest, "Optical fiber sensor technology," IEEE J. Quant. Electron. **QE-18**, 626–665 (1982).
[5] J. P. Goure, I. Verrier, and J. P. Meunier, "Linear and non-linear optical fibre devices," J. Phys. D: Appl. Phys. **22**, 1791–1805 (1989).
[6] D. L. Nelson and T. F. Krile, "A set of fiber optics experiments," IEEE Trans. Educ. **E-26**, 133–137 (1983).
[7] R. M. Bunch, "Optical fiber sensor experiments for the undergraduate physics laboratory," Am. J. Phys. **58**, 870–874 (1990).
[8] W. R. C. Rowley, "Interferometric measurements of length and distance," Alta Frequenza **XLI**, 887–896 (1972).
[9] H. C. Lefevre, "Single mode fractional wave device and polarisation controllers," Electron. Lett. **16**, 778–780 (1980).
[10] L. F. Stokes, M. Chodorow, and H. J. Shaw, "All single mode fiber resonator," Opt. Lett. **7**, 288–290 (1982).
[11] J. Wilson and J. F. B. Hawkes, *Optoelectronics: An Introduction* (Prentice-Hall, Englewood Cliffs, NJ, 1983).

An intuitive introduction to dual space and some simple physical applications

B. Lesche, I. Alcoforado, Jr., and M. L. Bedran
Instituto de Física, Universidade Federal do Rio de Janeiro, Ilha do Fundão—Bloco A, Rio de Janeiro, RJ 21945, Brazil

(Received 26 June 1991; accepted 6 December 1991)

A geometric and intuitive definition of dual vectors and some simple physical applications are given. Dual vectors are used in many branches of mathematics and physics on a high and less accessible level. It is shown that dual vectors are as simple and intuitive as ordinary vectors.

I. INTRODUCTION

Vectors are usually introduced in high school in an intuitive way and they are used in physics classes to represent velocity, force, displacement, and other entities. There exists other kinds of simple geometric objects called *dual vectors* or *linear functionals*. Usually dual vectors are introduced only in some special university courses and often in a much more abstract way. In this article we give an intuitive introduction to dual space and present some simple applications to physics.

Imagine the seats of the audience of a theater or cinema. We may describe the positions of the seats choosing one seat as an origin and pointing to all the other seats with position vectors. However, we may also look at the audience in a different—dual—way: Instead of paying attention to the individual seats we may recognize lines that form rows, columns, diagonals, etc. In the following we shall introduce the geometric objects that correspond to this dual way of looking and define mathematical operations with these objects.

II. DEFINITION OF DUAL VECTORS

A. Geometrical definition of dual vectors

Let us define a dual vector $\bar{a}$ as a point O together with a plane that does not contain the point O. We will call O the origin of $\bar{a}$ and call the plane the *characteristic plane of* $\bar{a}$. In the case of an n-dimensional space the characteristic plane of $\bar{a}$ would be an $(n-1)$-dimensional hyperplane. In two dimensions it is a straight line. (See Fig. 1.)

Ordinary vectors (often called free vectors) are considered identical if they differ only by a parallel transport. We shall assume the same in the case of dual vectors. (See Fig. 2.)

B. Sum of dual vectors

In order to construct the sum of two dual vectors $\bar{a}$ and $\bar{b}$, we first move one of them parallel to itself until the origins coincide. Then we draw two planes a' and b', parallel to the characteristic planes of $\bar{a}$ and $\bar{b}$, respectively, through the common origin. The sum of $\bar{a}$ and $\bar{b}$ is then given by the common origin together with the plane that contains the intersection of a' with the characteristic plane of $\bar{b}$ and the intersection of b' with the characteristic plane of $\bar{a}$. (See Fig. 3.)

This sum obviously obeys the rule $\bar{a}+\bar{b}=\bar{b}+\bar{a}$ (commutative law). It is also easy to verify that $(\bar{a}+\bar{b})+\bar{c}=\bar{a}+(\bar{b}+\bar{c})$ (associative law).

The attentive reader will note that the construction described above runs into difficulties when $\bar{a}$ and $\bar{b}$ are parallel. In this case, $(\bar{a}+\bar{b})$ can be constructed in the following way: First represent $\bar{a}$ as a sum of two dual vectors $\bar{a}_1$ and $\bar{a}_2$, which are not parallel to $\bar{b}$. Then $(\bar{a}+\bar{b})$ can be constructed as $\bar{a}_2+(\bar{a}_1+\bar{b})$ without any difficulty. We use this procedure to determine $\bar{a}+\bar{a}$. (See Fig. 4.)

Calling $\bar{a}+\bar{a}$ as usual $2\bar{a}$ one is motivated by this and similar examples to define:

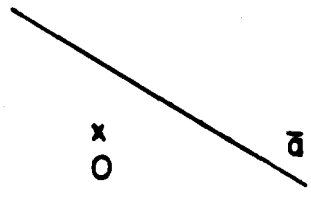

Fig. 1. A dual vector in two dimensions.